

# Anderson impurity model at finite Coulomb interaction $U$ : generalized Non-crossing Approximation

K. Haule<sup>1,2</sup>, S. Kirchner<sup>2</sup>, J. Kroha<sup>2</sup> and P. Wölfle<sup>2</sup>

<sup>1</sup>*J. Stefan Institute, SI-1000 Ljubljana, Slovenia*

<sup>2</sup>*Institut für Theorie der Kondensierten Materie, Universität Karlsruhe, D-76128 Karlsruhe, Germany*  
(December 2, 2024)

We present an extension of the non-crossing approximation (NCA), which is widely used to calculate properties of Anderson impurity models in the limit of infinite Coulomb repulsion  $U \rightarrow \infty$ , to the case of finite  $U$ . A self-consistent conserving pseudo-particle representation is derived by symmetrizing the usual NCA diagrams with respect to empty and doubly occupied local states. This requires an infinite summation of skeleton diagrams in the generating functional thus defining the “Symmetrized finite- $U$  NCA” (SUNCA). We show that within SUNCA the low energy scale  $T_K$  (Kondo temperature) is correctly obtained, in contrast to other simpler approximations discussed in the literature.

PACS numbers: 75.20.Hr, 71.27.+a, 71.15.-m, 71.10.-w

## I. INTRODUCTION

Anderson impurity models have been of considerable interest recently as generic models of local systems with internal degrees of freedom coupled to a Fermi gas. Although first introduced as models for magnetic impurities in metals<sup>1</sup>, they describe two-level systems in metals<sup>2</sup>, quantum dots in mesoscopic structures<sup>3,4</sup> and strongly correlated lattice systems in the local approximation of the Dynamic Mean Field Theory (DMFT)<sup>5</sup> as well. In a nutshell, the Anderson model features one or several local levels hybridizing with the conduction electron states of the metal. Multiple occupancy of the local levels is inhibited by the strong Coulomb repulsion  $U$  between electrons in the local states. As a consequence, the local levels are approximately singly occupied, giving rise to a magnetic moment or an equivalent degree of freedom. Due to the coupling to the conduction electron system, the local moment is screened<sup>1</sup>, or in a multi-channel situation forms a more complicated many-body state<sup>6</sup>.

Most investigations of Anderson models have concentrated on the case of infinite Coulomb repulsion  $U$ . The corresponding restriction of the local Hilbert space to electron occupation  $n_d \leq 1$  allows for an economical treatment in terms of pseudo-particle representations<sup>7,8</sup> and a projection onto the physical sector of Hilbert space. In this framework, the simplest approximation consists of second-order self-consistent perturbation theory in the hybridization, the so-called Non-Crossing Approximation (NCA)<sup>9,10</sup>. Although the NCA has its limitations, it is a valuable tool for extracting the complex many-body physics of Anderson impurity models. In the single channel case the NCA accounts correctly for the formation of a Kondo resonance at the Fermi level below the Kondo temperature  $T_K$ <sup>11</sup>, even though the appearance of a local Fermi liquid state at temperatures  $T \ll T_K$  is not captured in this approximation<sup>12</sup>. In the multichannel case even the correct low temperature power law behavior is obtained in NCA<sup>13</sup>. However, in order to capture, e.g.,

the physics of the upper and the lower Hubbard bands in a DMFT description of the Hubbard model and the Mott-Hubbard metal-insulator transition, it is essential to consider the case of large but finite  $U$ . It is therefore desirable to develop a generalization of NCA to the case of finite Coulomb interaction. In the following we present a straightforward generalization of NCA, which conserves the symmetry of virtual transitions to the empty local level or doubly occupied local level states. This is essential for recovering the correct Kondo temperature  $T_K$ , as pointed out by Pruschke and Grewe<sup>14</sup> and, as will be shown, requires an infinite summation of a certain class of crossing diagrams. We find that inclusion of only the first crossing term in this resummation<sup>14</sup>, while contributing the larger part of the change of  $T_K$ , is not sufficient to provide a qualitatively correct Kondo temperature.

## II. PSEUDOPARTICLE REPRESENTATION OF THE MODEL

The model we consider describes a local impurity level (called d-level in the following), hybridizing with the conduction electron states. The energy  $E_d$  of the level may be located below or above the Fermi energy. Two electrons with spins  $\uparrow$  and  $\downarrow$  on the local level experience a Coulomb interaction  $U$ . The local states will be assumed to be created by pseudo-particle operators  $f_\sigma^\dagger$  (singly occupied state with spin  $\sigma$ ),  $b^\dagger$  (empty state) and  $a^\dagger$  (doubly occupied state) acting on a vacuum state without any impurity. We choose  $f_\sigma$  to be fermion and  $a, b$  to be boson operators, where  $b$  will be called the “light” and  $a$  the “heavy” boson. The creation operator for the local physical electron can then be written as  $d_\sigma^\dagger = f_\sigma^\dagger b + \sigma a^\dagger f_{-\sigma}$ , where the pseudo-particle occupation numbers must satisfy the operator constraint

$$Q = a^\dagger a + b^\dagger b + \sum_{\sigma} f_{\sigma}^{\dagger} f_{\sigma} = 1, \quad (1)$$

expressing the fact that at any instant of time the impurity is in exactly one charge state, empty, singly, or doubly occupied, respectively. The fermion operators  $c_{\vec{k}\sigma}^\dagger$  create electrons in conduction electron states  $|\vec{k}\sigma\rangle$  with energy  $\epsilon_k$ . The Hamiltonian then takes the form

$$H = \sum_{\vec{k},\sigma} \epsilon_{\vec{k}} c_{\vec{k}\sigma}^\dagger c_{\vec{k}\sigma} + E_d(2a^\dagger a + \Sigma_\sigma f_\sigma^\dagger f_\sigma) + Ua^\dagger a + \sum_{\vec{k},\sigma} V(c_{\vec{k}\sigma}^\dagger b^\dagger f_\sigma + \sigma c_{\vec{k}\sigma}^\dagger f_{-\sigma}^\dagger a + h.c.), \quad (2)$$

where  $V$  is the hybridization matrix element. For later use we define the conduction electron density of states at the Fermi energy as  $\mathcal{N}(0)$  and the effective hybridization  $\Gamma = \pi\mathcal{N}(0)V^2$ .

### III. GAUGE SYMMETRY AND PROJECTION ONTO THE PHYSICAL HILBERT SPACE

The model described by the auxiliary particle Hamiltonian (2) is invariant under simultaneous, local  $U(1)$  gauge transformations,  $f_\sigma \rightarrow f_\sigma e^{i\phi(t)}$ ,  $b \rightarrow b e^{i\phi(t)}$ ,  $a \rightarrow a e^{i\phi(t)}$ , where  $\phi(t)$  is an arbitrary, time-dependent phase. This gauge symmetry guarantees the conservation of the local charge  $Q$  in time. In order to project onto the physical subspace  $Q = 1$ , it is therefore sufficient to carry out the projection at time  $t \rightarrow -\infty$ , if the gauge symmetry is implemented exactly. One starts with the grandcanonical ensemble with respect to  $Q$  and the associated chemical potential  $-\lambda$ . The projection is achieved by taking the limit  $\lambda \rightarrow \infty$  of any grandcanonical expectation value of a physical operator  $\hat{A}$  acting in the impurity Hilbert space

$$\langle \hat{A} \rangle = \lim_{\lambda \rightarrow \infty} \frac{\langle \hat{A} \rangle_G}{\langle \hat{Q} \rangle_G}. \quad (3)$$

Here the subscript  $G$  denotes the grandcanonical ensemble. The extra factor  $\hat{Q}$  in the denominator of Eq. (3) has been introduced to project out the  $Q = 0$  subspace. Note that in the numerator this factor can be omitted, since any physical operator  $\hat{A}$  acting on the impurity states consists of powers of  $d_\sigma^\dagger$ ,  $d_\sigma$ , which annihilate any state in the  $Q = 0$  subspace,  $d_\sigma^\dagger|Q = 0\rangle = 0$ ,  $d_\sigma|Q = 0\rangle = 0$ . A detailed description of the projection procedure is given in Ref.<sup>11</sup>. Expectation values in the grandcanonical ensemble may be calculated straightforwardly in perturbation theory in the hybridization  $V$ , making use of Wick's theorem. The usual resummation techniques may be applied. Thus the imaginary time single particle Green's functions

$$G_{f\sigma}(\tau_1 - \tau_2) = -\langle \hat{T}[f_\sigma(\tau_1) f_\sigma^\dagger(\tau_2)] \rangle_G \quad (4)$$

and analogously for the two bosons  $a, b$ , may be expressed in terms of the self-energies  $\Sigma_{f,b,c}(i\omega)$  as

$$\begin{aligned} G_{f\sigma}(i\omega) &= [i\omega - \lambda - E_d - \Sigma_f(i\omega)]^{-1} \\ G_b(i\omega) &= [i\omega - \lambda - \Sigma_b(i\omega)]^{-1} \\ G_a(i\omega) &= [i\omega - \lambda - 2E_d - U - \Sigma_a(i\omega)]^{-1}. \end{aligned} \quad (5)$$

The local conduction electron Green's function is given by

$$G_{c\sigma}(i\omega) = \left\{ \left[ G_{c\sigma}^0(i\omega) \right]^{-1} - \Sigma_{c\sigma}(i\omega) \right\}^{-1} \quad (6)$$

with

$$G_{c\sigma}^0(i\omega) = \sum_{\vec{k}} G_{c\sigma}^0(\vec{k}, i\omega) = \sum_{\vec{k}} [i\omega - \epsilon_k]^{-1}. \quad (7)$$

The physical d-electron Green's function is proportional to the single-particle conduction electron  $t$ -matrix  $t_{c\sigma}(i\omega)$ , and is related to the grandcanonical (unprojected)  $\Sigma_{c\sigma G}$  as

$$G_{d\sigma}(i\omega) = \frac{1}{V^2} t_{c\sigma}(i\omega) = \frac{1}{V^2} \lim_{\lambda \rightarrow \infty} e^{\beta\lambda} \Sigma_{c\sigma G}(i\omega, \lambda), \quad (8)$$

where  $\beta$  is the inverse temperature. The physical (projected onto the  $Q = 1$  subspace) local conduction electron self-energy is then obtained from the  $t$ -matrix as

$$\Sigma_{c\sigma}(i\omega) = \frac{V^2 G_{d\sigma}(i\omega)}{1 + V^2 G_{c\sigma}^0(i\omega) G_{d\sigma}(i\omega)}. \quad (9)$$

### IV. GENERATING FUNCTIONAL

Gauge invariant approximations conserving the local charge  $Q$  may be derived from a Luttinger–Ward generating functional  $\Phi$ . For a given approximation the functional  $\Phi$  is defined by a sum of closed skeleton diagrams. The self-energies  $\Sigma_\mu$ ,  $\mu = a, b, f, c$ , are obtained by taking the functional derivatives

$$\Sigma_\mu = \frac{\delta\Phi}{\delta G_\mu}. \quad (10)$$

The ‘‘Non-crossing Approximation’’ (NCA) in the limit  $U \rightarrow \infty$  is defined by the single lowest order diagram (2nd order in  $V$ ) containing a light boson line (the first diagram of Fig. 1). In the limit of small hybridization element  $V_{\vec{k}}$ , it appears to be justified to keep only the lowest order contribution in  $V$ . However, as discussed in Refs.<sup>12,16</sup>, the singular behavior of vertex functions may require to include these as well. This turns out to be necessary in the single channel model where the formation of a many-body resonance state is essential for recovering the Fermi liquid behavior, and less so in the multi-channel models. Including an infinite class of skeleton diagrams in  $\Phi$  (in a ‘‘Conserving T-matrix Approximation’’ (CTMA)), which allows to capture a singular structure in the spin and charge excitation sectors, the

low temperature Fermi liquid phase of the single channel Anderson model is recovered<sup>12</sup>.

Here we are interested in constructing a simpler generalization of NCA to describe the case of finite  $U$ . It seems straightforward to define such an approximation by adding to the second order skeleton diagram for  $\Phi$  containing the light boson (the first diagram in Fig. 1 a)) the corresponding diagram containing the heavy boson (the second diagram in Fig. 1 a)). This approximation has been considered sometime ago<sup>14,19</sup>, where it was found to fail badly: not even the Kondo energy scale is recovered in the so-defined approximation. The reason for this failure is obvious<sup>14,19</sup>: In the Kondo regime ( $n_d \lesssim 1$ ) the local spin is coupled to the conduction electron spin density at the impurity through the antiferromagnetic exchange coupling

$$J = V^2 \left( -\frac{1}{E_d} + \frac{1}{E_d + U} \right). \quad (11)$$

The two terms on the r.h.s. of this relation arise from virtual transitions into the empty and doubly occupied local level, which e.g. contribute equally in the symmetric case  $|E_d| = E_d + U$ . The symmetric occurrence of these two virtual processes in all intermediate states is not included in the simple extension of NCA proposed above. Rather, the self-energy insertions in each of the two diagrams contain always only one of the processes, leading to an effective  $J$  which is only one half of the correct value. Correspondingly, the Kondo temperature  $T_K \sim \exp[-1/(2N(0)J)]$  comes out to scale as the square of the correct value, which can be orders of magnitude too small.

To correct this deficiency it is necessary to include additional diagrams, restoring the symmetry between the two virtual processes. As a first step one may add the next order skeleton diagram to  $\Phi$  (Fig. 1 b)). As we will show below, this approximation, later referred to as UNCA, helps to recover a large part of the correct behavior of  $T_K$ <sup>14</sup>. However, as seen from the preceding discussion, for a completely symmetric treatment of empty and doubly occupied intermediate states one must first consider the diagrams of bare perturbation theory instead of skeleton diagrams. A symmetric class of diagrams is generated by replacing a light boson line with a heavy boson line in each of the bare (non-skeleton) diagrams comprising the NCA, and vice versa. Each replacement leads to a crossing of conduction electron lines spanning one fermion and at most two boson lines. A conserving approximation is then constructed by substituting renormalized propagators for the bare ones and keeping only skeleton diagrams. The resulting generating functional  $\Phi$  is shown diagrammatically in Fig. 1 a)–c).

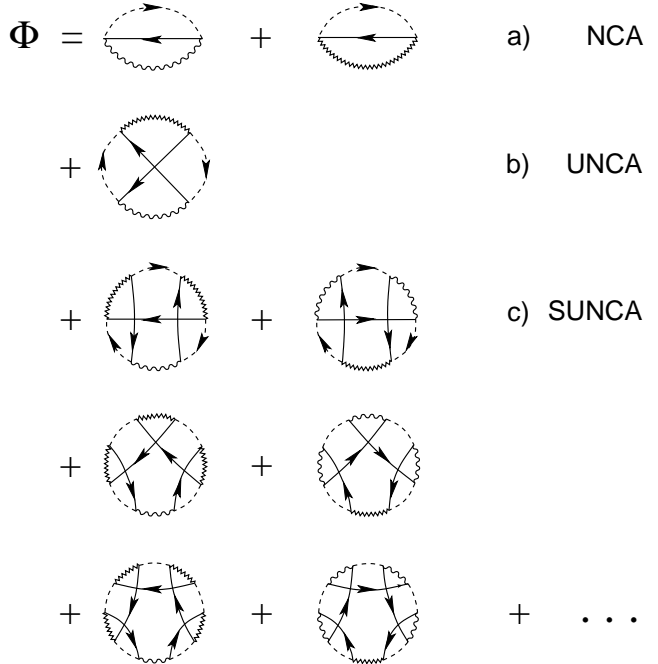


FIG. 1. Diagrammatic representation of the generating functional to describe the Anderson impurity model at finite  $U$ . Throughout this paper, solid, dashed, wiggly and zig-zag lines correspond to conduction electron  $c$ , pseudo-fermion  $f$ , light boson  $b$ , and heavy boson  $a$  propagators, respectively. a) NCA including light and heavy boson lines. a)–b) Finite- $U$  NCA (UNCA). This approximation amounts to renormalizing only one of the vertices in each of the self-energy diagrams of Fig. 2 and keeping only one (light or heavy boson) rung in the corresponding vertex function (see text). a)–c) Symmetrized finite- $U$  NCA (SUNCA).

These diagrams look similar to the CTMA diagrams mentioned above, but contain one light boson line and an arbitrary number of heavy boson lines, or vice versa. Diagrams with, for example, two light boson lines and an arbitrary number of heavy boson lines (and conduction electron lines spanning at most one fermion line) are reducible and do not appear. We will call the approximation defined by the generating functional given by the sum of the diagrams of Fig 1 “Symmetrized finite- $U$  NCA” (SUNCA). The above approximation corresponding to the CTMA at  $U \rightarrow \infty$ , termed “Symmetrized finite- $U$  Conserving T-matrix Approximation” (SUCTMA) is thus defined in a natural way by summing up all skeleton  $\Phi$  diagrams containing a single closed ring of auxiliary particle propagators with an arbitrary number of light or heavy boson lines, dressed by conduction electron lines spanning only one fermion line. Thus, the SUCTMA is defined by adding to the diagrams of the SUNCA the CTMA diagrams with (only) light boson lines or (only) heavy boson lines. The SUCTMA equations have not yet been evaluated.

## V. RESULTS OF SUNCA

As discussed above, the self-energies  $\Sigma_\mu$  are obtained by functional differentiation of the generating functional with respect to the Green's functions  $G_\mu$ . The functional  $\Phi$  defined by Fig. 1 leads to an infinite series of diagrams for  $\Sigma_\alpha$ , which may be conveniently presented in terms of three-point vertex functions (the filled semicircles with three legs: one boson and two fermion lines), see Fig. 2. It is necessary to subtract a diagram of 4th order in  $V$  in each case to avoid double counting. On the level of SUNCA and SUCTMA the vertex functions consist of ladder summations, with light or heavy boson lines as rungs, and are defined diagrammatically in Fig. 3. Note that keeping only a single light or heavy boson rung in these vertex functions corresponds to UNCA.

$$\begin{aligned}
 \Sigma_b &= \text{diagram 1} + \text{diagram 2} - \text{diagram 3} \\
 \Sigma_a &= \text{diagram 1} + \text{diagram 2} - \text{diagram 3} \\
 \Sigma_f &= \text{diagram 1} + \text{diagram 2} - 2 \text{diagram 3} \\
 V^2 G_d &= \text{diagram 1} + \text{diagram 2} - 2 \text{diagram 3}
 \end{aligned}$$

FIG. 2. Diagrammatic representation of the auxiliary particle self-energies of SUNCA in terms of the renormalized hybridization vertices, defined in Fig. 3. In each line the third diagram is subtracted in order to avoid double counting of terms within the first two diagrams.

The expressions for the self-energies  $\Sigma_\mu$  defined by Figs. 2 and 3, together with the definition of the Green's functions, Eqs. (5), constitute a set of nonlinear integral equations for  $\Sigma_\mu(\omega)$ ,  $\mu = a, b, f$ . The local conduction electron self-energy  $\Sigma_c$  does not appear in any internal Green's functions because it contains at least one auxiliary particle loop, i.e. carries a factor  $\exp(-\beta\lambda)$  and thus

$$\begin{aligned}
 \text{a) } & \text{diagram 1} = \text{diagram 2} + \text{diagram 3} \\
 \text{b) } & \text{diagram 1} = \text{diagram 2} + \text{diagram 3}
 \end{aligned}$$

FIG. 3. Diagrammatic representation of the Bethe-Salpeter equations for a) the renormalized light boson (empty impurity) and b) the renormalized heavy boson (doubly occupied impurity) vertex, as generated by the SUNCA Luttinger-Ward functional (Fig. 1).

vanishes due to the exact projection onto the physical Hilbert space ( $\lambda \rightarrow \infty$ )<sup>11</sup>.  $G_d$  and therefore  $\Sigma_c$  may be calculated at the end via Eqs. (8), (9) by using the self-consistently determined  $G_\alpha$ ,  $\alpha = a, b, f$ . The SUNCA equations are given explicitly in appendix A. Although these equations are more involved than the regular NCA, they are numerically considerably more easily tractable than the CTMA equations<sup>12,16</sup>, since SUNCA contains only renormalized three-point vertices (see Fig. 2) as compared to four-point vertex functions occurring in CTMA<sup>12</sup>. We solved the SUNCA equations numerically in the real frequency representation, i.e. after analytic continuation from Matsubara frequencies  $\omega_n$  to the real frequency axis.

As a first important characteristic feature of the pseudo-particles we note that the single-particle excitation spectrum is powerlaw divergent,  $G_\mu(\omega) \sim \omega^{-\alpha_\mu}$ ,  $\mu = a, b, f$  reflecting the abundance of low energy excitations forced by the constraint. At finite temperature  $T$  these singularities are cut off at the scale  $\omega \sim T$ . As observed in earlier work<sup>12,17</sup>, the values of the exponents  $\alpha_\mu$  are characteristic of the state of the system. In the single channel case, when the ground state is a local Fermi liquid, the exponents may be inferred from the Friedel sum

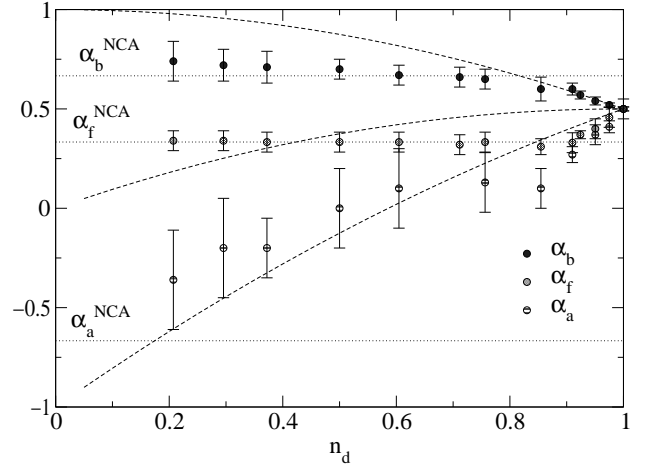


FIG. 4. Infrared threshold exponents of the auxiliary particle spectral functions  $-\text{Im}G_{f,a,b}^R(\omega)/\pi$ , in dependence of the impurity occupation  $n_d$ , for fixed values of  $\Gamma$  and  $U$  and varying  $E_d$ . Dashed curved lines: exact results (Eq. (12)); horizontal lines: NCA results; data points with error bars: SUNCA results. In the Kondo limit ( $n_d \rightarrow 1$ ) the exact exponents are recovered, while in the mixed valence and empty impurity regime the SUNCA results for  $\alpha_f$  and  $\alpha_b$  cross over to the NCA values.

rule relating the scattering phase shifts  $\eta_{\mu,\sigma}$  to the number of electrons bound to the impurity in each channel  $\Delta n_{\mu,\sigma} = \eta_{\mu,\sigma}/\pi$ . The exponents  $\alpha_\mu$  in turn are related to the  $\eta_{\mu,\sigma}$  by the general result first derived for the x-ray edge singularities<sup>18</sup>,  $\alpha_\mu = 1 - \sum_\sigma (\eta_{\mu\sigma}/\pi)^2$ . This is so, since e.g. the heavy boson Green's function, describing

the transition amplitude for a doubly occupied impurity to be created at time  $t = 0$  and removed at a later time is proportional to the overlap of the free Fermi sea of conduction electrons with the ground state of the Anderson model. The change in the occupation of the local level due to the hybridization with the conduction band  $\Delta n_{\mu\sigma}$  is the difference between the  $t = 0$  initial impurity occupation  $n_{\mu\sigma}(t = 0)$  (without hybridization) and the occupation in the ground state of the Anderson impurity model  $n_{d\sigma} = n_d/2$ , i.e. it depends on the initial conditions of the different Green's functions  $G_\mu$ ,  $\mu = a, b, f$ . Thus we have  $\Delta n_{a,\sigma} = \frac{2-n_d}{2}$ ,  $\Delta n_{f,\sigma} = \delta_{\sigma,\sigma_0} - \frac{1}{2}n_d$  (where  $\sigma_0$  is the spin of the fermion in the Green's function  $G_{f\sigma_0}$ ), and  $\Delta n_{b,\sigma} = -\frac{n_d}{2}$ . The infrared threshold exponents of  $G_\mu(\omega)$  are therefore given by

$$\begin{aligned}\alpha_a &= -1 + 2n_d - \frac{n_d^2}{2} \\ \alpha_b &= 1 - \frac{n_d^2}{2} \\ \alpha_f &= n_d - \frac{n_d^2}{2}.\end{aligned}\quad (12)$$

In Fig. 4 we show the exponents  $\alpha_\mu$  for different  $n_d$ , as obtained from a numerical solution of the SUNCA equations. Also shown is the exact result given by Eq. (12) (dashed lines), and the analytical result that can be extracted analytically from the NCA equations (defined by the first two diagrams in Fig. 1) in analogy to Ref.<sup>15</sup>. The numerical results of SUNCA (data points) are seen to approach the exact result in the limit  $n_d \rightarrow 1$ , but in the case of  $\alpha_b$  and  $\alpha_f$  appear to follow the NCA result rather than the exact result for  $n_d \leq 0.8$ . The results

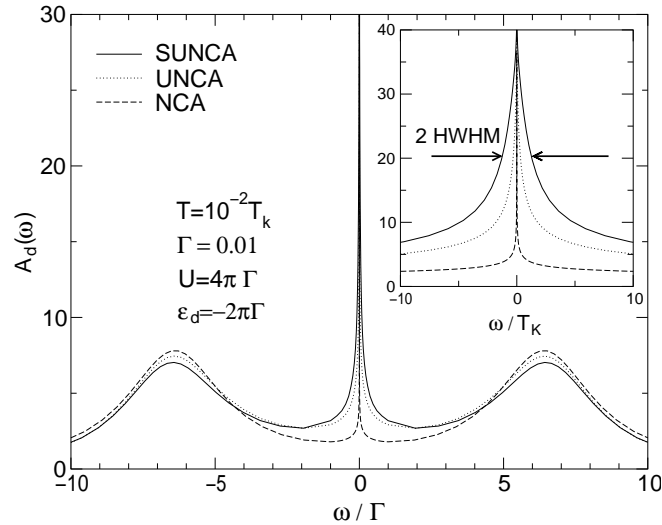


FIG. 5. Local electron spectral function calculated using NCA, UNCA, and SUNCA. The Kondo temperature is determined as the HWHM of the Kondo peak (see inset). It is seen that in NCA the Kondo peak width comes out orders of magnitude too low.

for the exponent  $\alpha_a$  trace the exact behavior in reasonable agreement. Clearly the SUNCA does much better than the simple NCA. From our experience<sup>12</sup> with the Anderson model in the limit  $U \rightarrow \infty$ , we expect that the correct exponents should be recovered in SUCTMA.

We now turn to the d-electron spectral function  $A_d(\omega) = \frac{1}{\pi} \text{Im} G_d(\omega - i0)$ . Fig. 5 shows the results for  $A_d(\omega)$  for the symmetric Anderson model in the Kondo regime ( $n_d \approx 1$ ) at a very low temperature of  $T \simeq 10^{-2} T_K$ . Shown are the results obtained from the simple NCA (diagrams of first line in Fig. 1), the perturbatively corrected version UNCA (including the diagram in the second line of Fig. 1) and the full SUNCA. The inset shows that the width of the Kondo resonance peak, which is a measure of  $T_K$ , comes out orders of magnitude different in the three approximations. In order to compare the numerical results with the exact expression for  $T_K$ ,

$$T_K = \min \left\{ \frac{1}{2\pi} U \sqrt{I}, \sqrt{D\Gamma} \right\} e^{-\pi/I} \quad (13)$$

where

$$I = 2 \left[ \frac{\Gamma}{|E_d|} + \frac{\Gamma}{E_d + U} \right], \quad (14)$$

we determine  $T_K$  as the half width of the Kondo resonance at half maximum (HWHM).

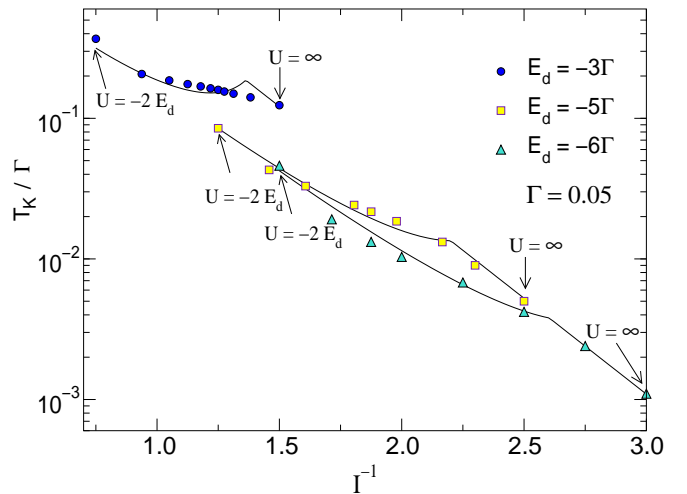


FIG. 6. Kondo Temperature for various parameters  $E_d$ ,  $U$  and fixed  $\Gamma$ . Solid lines represent the exact results, Eqs. (13), (14). Data points are the SUNCA results determined from the width of the Kondo peak in the d-electron spectral function.

In Fig. 6 the results for  $T_K/\Gamma$  obtained in this way for a fixed value of  $\Gamma = 0.05$  (in units of  $D$ ) and several values of  $E_d/\Gamma$ , as a function of  $I(U/\Gamma)$  (data points) are compared with the exact values Eqs. (13), (13) (solid lines). The agreement is excellent, demonstrating that the SUNCA provides the correct scale  $T_K$  for a wide range of parameters  $E_d$  and  $U$ .

## VI. CONCLUSION

In this paper we have proposed a conserving scheme to describe the Anderson impurity model at finite on-site repulsion  $U$  within the auxiliary particle method. In order to incorporate the correct value of the spin exchange coupling  $J$  into the theory and, hence, to obtain the correct size of the low-energy scale  $T_K$ , it is necessary to treat fluctuation processes into the empty and into the doubly occupied intermediate state on equal footing at the level of bare perturbation theory. The simplest Luttinger–Ward functional which is completely symmetric in this respect consists of an infinite series of skeleton diagrams, corresponding to ladder-type vertex renormalizations in the self-energies. Although considerably more involved than the regular NCA, this approximation, termed “symmetrized finite- $U$  NCA” (SUNCA), is numerically tractable on a typical workstation. We

find that SUNCA recovers the correct Kondo temperature over a wide range of the parameters of the Anderson model  $E_d$ ,  $U$ , and  $\Gamma$ , while simplified approximations (NCA, UNCA) produce a low-energy scale typically orders of magnitude smaller than the exact value. This result is especially relevant for a correct description of the low temperature properties of strongly correlated lattice models by a diagrammatic many-body technique, since in the limit of infinite dimensions these models reduce to a selfconsistent, finite- $U$  single-impurity problem. Applications of the present theory to such models are currently in progress.

We are grateful to T. A. Costi and Th. Pruschke for useful discussions. This work was supported by DFG through Sonderforschungsbereich 195 (S.K., J.K., P.W.) and by the ESF program “Fermi liquid instabilities in correlated metals” (FERLIN).

## APPENDIX A: SUNCA EQUATIONS

In this appendix we explicitly give the self-consistent SUNCA equations which, together with the definitions Eqs. (5) of the Green’s functions, determine the auxiliary particle self-energies. We also give the expression for the physical d-electron spectral function in terms of

the auxiliary particle propagators.

We first define the ladder vertex functions  $T_a$ ,  $T_b$  with heavy boson  $a$  and light boson  $b$  rungs, respectively, as shown diagrammatically in Fig. 3. These vertex functions, projected onto the physical subspace  $Q = 1$  and analytically continued to real frequencies, obey the following Bethe–Salpeter equations,

$$T_{a\sigma}(\omega, \Omega) = \Gamma \int \frac{d\epsilon}{\pi} f(\epsilon - \Omega) A_{c-\sigma}^0(\epsilon - \Omega) G_{f-\sigma}(\epsilon) G_a(\epsilon + \omega - \Omega) + \Gamma \int \frac{d\epsilon}{\pi} f(\epsilon - \Omega) A_{c-\sigma}^0(\epsilon - \Omega) G_{f-\sigma}(\epsilon) G_a(\epsilon + \omega - \Omega) T_{a-\sigma}(\epsilon, \Omega) \quad (\text{A1})$$

$$T_{b\sigma}(\omega, \Omega) = \Gamma \int \frac{d\epsilon}{\pi} f(\epsilon - \Omega) A_{c\sigma}^0(\Omega - \epsilon) G_{f-\sigma}(\epsilon) G_b(\epsilon + \omega - \Omega) + \Gamma \int \frac{d\epsilon}{\pi} f(\epsilon - \Omega) A_{c\sigma}^0(\Omega - \epsilon) G_{f-\sigma}(\epsilon) G_b(\epsilon + \omega - \Omega) T_{b-\sigma}(\epsilon, \Omega), \quad (\text{A2})$$

where  $f(\epsilon)$  is the Fermi function,  $A_{c\sigma}^0(\epsilon) = \frac{1}{\pi} \text{Im} G_{c\sigma}^0(\epsilon) / \mathcal{N}(0)$  the bare conduction electron density of states per spin, normalized to the density of states at

the Fermi level and, for concreteness, all propagators are to be understood as the advanced ones. The auxiliary particle self-energies (Fig. 2) are then given by,

$$\Sigma_{f\sigma}(\omega) = \Gamma \int \frac{d\epsilon}{\pi} f(\epsilon - \omega) A_{c\sigma}^0(\omega - \epsilon) G_b(\epsilon) [1 + T_{a\sigma}(\omega, \epsilon)]^2 + \Gamma \int \frac{d\epsilon}{\pi} f(\epsilon - \omega) A_{c-\sigma}^0(\epsilon - \omega) G_a(\epsilon) [1 + T_{b\sigma}(\omega, \epsilon)]^2 - 2\Gamma^2 \int \frac{d\epsilon}{\pi} f(\epsilon - \omega) A_{c\sigma}^0(\omega - \epsilon) G_b(\epsilon) \int \frac{d\epsilon'}{\pi} f(\epsilon' - \epsilon) A_{c-\sigma}^0(\epsilon' - \epsilon) G_{f-\sigma}(\epsilon') G_a(\epsilon' + \omega - \epsilon) \quad (\text{A3})$$

$$\Sigma_b(\omega) = \Gamma \sum_{\sigma} \int \frac{d\epsilon}{\pi} f(\epsilon - \omega) A_{c\sigma}^0(\epsilon - \omega) G_{f\sigma}(\epsilon) [1 + T_{a\sigma}(\epsilon, \omega)] + \Gamma^2 \sum_{\sigma} \int \frac{d\epsilon}{\pi} f(\epsilon - \omega) A_{c\sigma}^0(\epsilon - \omega) G_{f\sigma}(\epsilon) \times \int \frac{d\epsilon'}{\pi} f(\epsilon' - \omega) A_{c-\sigma}^0(\epsilon' - \omega) G_{f-\sigma}(\epsilon') G_a(\epsilon' + \epsilon - \omega) \{ [1 + T_{b\sigma}(\epsilon, \epsilon' + \epsilon - \omega)] [1 + T_{b-\sigma}(\epsilon', \epsilon' + \epsilon - \omega)] - 1 \} \quad (\text{A4})$$

$$\begin{aligned}
\Sigma_a(\omega) = & \Gamma \sum_{\sigma} \int \frac{d\epsilon}{\pi} f(\epsilon - \omega) A_{c-\sigma}^0(\omega - \epsilon) G_{f\sigma}(\epsilon) [1 + T_{b\sigma}(\epsilon, \omega)] \\
& + \Gamma^2 \sum_{\sigma} \int \frac{d\epsilon}{\pi} f(\epsilon - \omega) A_{c-\sigma}^0(\omega - \epsilon) G_{f\sigma}(\epsilon) \times \\
& \int \frac{d\epsilon'}{\pi} f(\epsilon' - \omega) A_{c\sigma}^0(\omega - \epsilon') G_{f-\sigma}(\epsilon') G_b(\epsilon' + \epsilon - \omega) \{ [1 + T_{a\sigma}(\epsilon, \epsilon' + \epsilon - \omega)] [1 + T_{a-\sigma}(\epsilon', \epsilon' + \epsilon - \omega)] - 1 \}.
\end{aligned} \tag{A5}$$

In order to calculate the physical impurity electron spectral function  $A_{d\sigma}$  from the selfconsistently determined  $G_a$ ,  $G_b$ ,  $G_f$ , it is convenient to define modified vertex functions as

$$S_{a\sigma}^R(\omega, \Omega) = 1 + \Gamma \int \frac{d\epsilon}{\pi} f(\epsilon - \Omega) A_{c\sigma}^0(\epsilon - \Omega) \operatorname{Re}\{G_{f\sigma}(\epsilon)[1 + T_{a\sigma}(\epsilon, \Omega)]\} G_a(\epsilon + \omega) \tag{A6}$$

$$S_{a\sigma}^I(\omega, \Omega) = 1 + \Gamma \int \frac{d\epsilon}{\pi} f(\epsilon - \Omega) A_{c\sigma}^0(\epsilon - \Omega) \operatorname{Im}\{G_{f\sigma}(\epsilon)[1 + T_{a\sigma}(\epsilon, \Omega)]\} G_a(\epsilon + \omega) \tag{A7}$$

$$S_{b\sigma}^R(\omega, \Omega) = 1 + \Gamma \int \frac{d\epsilon}{\pi} f(\epsilon - \Omega) A_{c-\sigma}^0(\Omega - \epsilon) \operatorname{Re}\{G_{f\sigma}(\epsilon)[1 + T_{b\sigma}(\epsilon, \Omega)]\} G_b(\epsilon - \omega) \tag{A8}$$

$$S_{b\sigma}^I(\omega, \Omega) = 1 + \Gamma \int \frac{d\epsilon}{\pi} f(\epsilon - \Omega) A_{c-\sigma}^0(\Omega - \epsilon) \operatorname{Im}\{G_{f\sigma}(\epsilon)[1 + T_{b\sigma}(\epsilon, \Omega)]\} G_b(\epsilon - \omega). \tag{A9}$$

The impurity spectral function then reads

$$\begin{aligned}
A_{d\sigma}(\omega) = & -\frac{1}{\pi} \operatorname{Im} \int \frac{d\Omega}{\pi} \frac{e^{-\beta\Omega}}{f(-\omega)} G_{f\sigma}(\Omega + \omega) \{ \operatorname{Im}[G_b(\Omega)] [S_{a-\sigma}^R(\omega, \Omega)^2 - S_{a-\sigma}^I(\omega, \Omega)^2] + 2\operatorname{Re}[G_b(\Omega)] S_{a-\sigma}^R(\omega, \Omega) S_{a-\sigma}^I(\omega, \Omega) \} \\
& -\frac{1}{\pi} \operatorname{Im} \int \frac{d\Omega}{\pi} \frac{e^{-\beta\Omega}}{f(\omega)} G_{f-\sigma}(\Omega - \omega) \{ \operatorname{Im}[G_a(\Omega)] [S_{b\sigma}^R(\omega, \Omega)^2 - S_{b\sigma}^I(\omega, \Omega)^2] + 2\operatorname{Re}[G_a(\Omega)] S_{b\sigma}^R(\omega, \Omega) S_{b\sigma}^I(\omega, \Omega) \} \\
& + 2\frac{\Gamma}{\pi} \int \frac{d\Omega}{\pi} \frac{e^{-\beta\Omega}}{f(\omega)} \int \frac{d\epsilon}{\pi} f(\epsilon - \Omega) A_{c-\sigma}^0(\epsilon - \Omega) \operatorname{Im}[G_b(\Omega) G_{f-\sigma}(\epsilon)] \operatorname{Im}[G_{f\sigma}(\Omega + \omega) G_a(\epsilon + \omega)].
\end{aligned} \tag{A10}$$

Note that the exponential divergencies of the statistical factors appearing in Eq. (A10) are compensated by the threshold behavior of the corresponding auxiliary particle spectral functions  $A_{\mu}(\omega) = \frac{1}{\pi} \operatorname{Im} G_{\mu}(\omega)$ ,  $\mu = a, b, f$  in the integrands. For the numerical treatment, these divergencies can be explicitly absorbed by formulating the self-consistency equations (A1)–(A10) in terms of the

functions  $\tilde{A}_{\mu}(\omega)$  which are defined via

$$A_{\mu}(\omega) = f(-\omega) \tilde{A}_{\mu}(\omega) \tag{A11}$$

and, hence, have no exponential divergence. We thus have, e.g.,  $\exp(-\beta\omega) A_{\mu}(\omega) = f(\omega) \tilde{A}_{\mu}(\omega)$ . Details of this representation are described in Ref.<sup>11</sup>.

<sup>1</sup> A.C. Hewson, “The Kondo Problem to Heavy Fermions”, (Cambridge University Press, 1993).

<sup>2</sup> D.L. Cox and A. Zawadowski, Adv. Phys. **47**, 599 (1998).

<sup>3</sup> T. K. Ng and P. A. Lee, Phys. Rev. Lett. **61**, 1768 (1988).

<sup>4</sup> L. I. Glazman and M. E. Raikh, Pis'ma Zh. Eksp. Teor. Fiz. **47**, 378 (1999) [JETP Lett. **47**, 452 (1988)].

<sup>5</sup> A. Georges, G. Kotliar, W. Krauth and M.J. Rozenberg, Rev. Mod. Phys. **68**, 13 (1996).

<sup>6</sup> N. Andrei and C. Destri, Phys. Rev. Lett. **52**, 364 (1984).

<sup>7</sup> S.E. Barnes, J. Phys. F **6**, 1375 (1976); **7**, 2637 (1977).

<sup>8</sup> P. Coleman, Phys. Rev. B **29**, 3035 (1984).

<sup>9</sup> H. Keiter and J.C. Kimball, J. Appl. Phys. **42**, 1460 (1971); N. Grewe and H. Keiter, Phys. Rev. B **24**, 4420 (1981).

<sup>10</sup> Y. Kuramoto, Z. Phys. B **53**, 37 (1983).

<sup>11</sup> T. A. Costi, J. Kroha, and P. Wölfle, Phys. Rev. B **53**, 1850 (1996).

<sup>12</sup> J. Kroha, P. Wölfle, and T. A. Costi, Phys. Rev. Lett. **79**, 261 (1997).

<sup>13</sup> D. L. Cox and A. E. Ruckenstein, Phys. Rev. Lett. **71**, 1613 (1993).

<sup>14</sup> Th. Pruschke and N. Grewe, Z. Phys. B **74**, 439 (1989).

<sup>15</sup> B. Menge and E. Müller-Hartmann, Z. Phys. B **73**, 225 (1988).

<sup>16</sup> J. Kroha and P. Wölfle, Proceedings of the International Conference on “Mathematical Methods in Physics”, Montreal 2000, D. Senechal, ed. (Springer, in press); J. Kroha and P. Wölfle, Acta Phys. Pol. B **29** (12), 3781 (1998).

<sup>17</sup> T. A. Costi, P. Schmitteckert, J. Kroha, and P. Wölfle, Phys. Rev. Lett. **73**, 11275 (1994); Physica C **235-240**, 2287 (1994); T. Schauerer, J. Kroha, and P. Wölfle, Phys. Rev. B **62**, 4394 (2000).

<sup>18</sup> P. Nozierès and C. T. DeDominicis, Phys. Rev. **178**, 1073; 1084; 1097 (1969).

<sup>19</sup> I. Holm and K. Schönhammer, Solid State Comm. **69**, 10, 969 (1989).